THE JOURNAL OF BIOLOGICAL CHEMISTRY VOL. 286, NO. 7, pp. 5540–5545, February 18, 2011
© 2011 by The American Society for Biochemistry and Molecular Biology, Inc. Printed in the U.S.A.

Analysis of Heterotropic Cooperativity in Cytochrome P450 3A4 Using α-Naphthoflavone and Testosterone*[S]

Received for publication, September 5, 2010, and in revised form, December 21, 2010 Published, JBC Papers in Press, December 22, 2010, DOI 10.1074/jbc.M110.182055

Daniel J. Frank, Ilia G. Denisov, and Stephen G. Sligar[1]

From the Department of Biochemistry, School of Molecular and Cellular Biology, University of Illinois, Urbana, Illinois 61801

Cytochrome P450 3A4 (CYP3A4) displays non-Michaelis-Menten kinetics for many of the substrates it metabolizes, including testosterone (TST) and α-naphthoflavone (ANF). Heterotropic effects between these two substrates can further complicate the metabolic profile of the enzyme. In this work, monomeric CYP3A4 solubilized in Nanodiscs has been studied for its ability to interact with varying molar ratios of ANF and TST. Comparison of the observed heme spin state, NADPH consumption, and product formation rates with a non-cooperative model calculated from a linear combination of the global analysis of each substrate reveals a detailed landscape of the heterotropic interactions and indicates negligible binding cooperativity between ANF and TST. The observed effect of ANF on the kinetics of TST metabolism is due to the additive action of the second substrate with no specific allosteric effects.

Hepatic cytochromes P450 play a fundamental role in the breakdown of xenobiotics from the blood. The most abundant of these in the adult human liver is cytochrome P450 3A4 (CYP3A4)[2] (1), which metabolizes approximately half of the most commonly prescribed drugs (2). Its ability to interact simultaneously with multiple substrate molecules leads to atypical kinetic phenomena, termed homotropic or heterotropic cooperativity (3–6), the former describing interactions of molecules of the same substrate and the latter referring to interactions of different substrates. Evidence of CYP3A4 simultaneously interacting with multiple substrate molecules comes from the crystal structures of the enzyme, which show a large, plastic active site (7), substrate bound at a peripheral binding site (8), changes in kinetic behavior in the presence of so-called effector molecules (9–12), as well as a global analysis of multiple observable enzyme properties (13–16).

Recent work from our laboratory has shown that the apparent heterotropic cooperativity in Type I spin transition between ANF and TST can be accounted for by the additive effect of the ability of each substrate to induce the spin transition (17). Differences in their relative spectral affinities may give the appearance of a stimulatory effect of ANF on TST-induced spin transition; however, this is not indicative of any true cooperative behavior in binding (17). Here, we extend this analysis to include the contributions of NADPH oxidation and product-forming rates from each of the substrates to elucidate a more complete understanding of the heterotropic interactions of this important drug-metabolizing enzyme.

EXPERIMENTAL PROCEDURES

Chemicals—Imidazole, sodium cholate, ANF, TST, and Amberlite were purchased from Sigma-Aldrich, CHAPS was purchased from Anatrace Inc. (Maumee, OH), Emulgen 913 was from Karlan Research Products Corp. (Santa Rosa, CA), palmitoyloleoylphosphatidylcholine was from Avanti Polar Lipids Inc. (Alabaster, AL), and 2β-, 6β-, and 15β-OH TST were from Steraloids, Inc. (Newport, RI). All other chemicals were purchased from Fisher Scientific and were at least ACS grade.

Expression, Purification, and Nanodisc Assembly—Cytochrome P450 3A4 was expressed from the NF-14 construct in the PCWori+ vector with a C-terminal pentahistidine tag generously provided by Dr. F. P. Guengerich (Vanderbilt University, Nashville, TN). Heterologous expression and purification from *Escherichia coli* and incorporation into Nanodiscs were carried out as described previously (17–20). Assembly of CYP3A4 in Nanodiscs was accomplished using the membrane scaffold protein MSP1D1 after removal of its histidine tag. Purified CYP3A4 from the *E. coli* expression system was solubilized by 0.1% Emulgen 913 and mixed with a disk reconstitution mixture containing MSP1D1, palmitoyloleoylphosphatidylcholine, and sodium cholate present in 1:10:650 molar ratios, respectively. Detergents were removed by treatment with Amberlite beads, initiating a self-assembly process. The discs were purified over a Sephadex G-200 size exclusion column and a nickel-nitrilotriacetic acid column. Fractions were examined for bromocriptine binding, and those that did not show a ≥85% spin conversion at a saturating concentration were discarded. The remaining pooled fractions showed a minimum 90% spin conversion. Cytochrome P450 reductase was expressed using the rat cytochrome P450 reductase/pOR262 plasmid, a generous gift from Dr. Todd D. Porter (University of Kentucky, Lexington, KY). Expression and purification of cytochrome P450 reductase from *E. coli* were performed as described previously (16, 19).

UV-visible Spectroscopy—Studies were performed at 3 μM CYP3A4 in Nanodiscs using a Cary 300 spectrophotometer (Varian, Lake Forest, CA) at 37 °C, with correction for substrate partitioning into the lipid bilayer as described previ-

* This work was supported, in whole or in part, by National Institutes of Health Grants GM31756 and GM33775 (to S. G. S.).

[S] The on-line version of this article (available at http://www.jbc.org) contains supplemental text and equations.

[1] To whom correspondence should be addressed: Dept. of Biochemistry, 116 Morrill Hall, University of Illinois, 505 South Goodwin Ave., Urbana, IL 61801. Fax: 217-265-4073; E-mail: s-sligar@uiuc.edu.

[2] The abbreviations used are: CYP3A4, cytochrome P450 3A4; TST, testosterone; ANF, α-naphthoflavone.

ously (17, 21), using partition coefficients, $K_p = 3000$ and 500 for ANF and TST, respectively. For the 1:3 ANF:TST mixed titration, a 1:1.7 ratio of substrates was prepared and added to the CYP3A4-Nanodisc solution, thereby maintaining the substrate ratio at 1:3 in the aqueous phase. The final concentration of methanol was never higher than 1%.

NADPH Oxidation and Product Formation—CYP3A4 incorporated Nanodiscs with cytochrome P450 reductase in a 1:3.5 molar ratio, and substrates were preincubated for 3 min at 37 °C in a 1-ml reaction volume in 100 mM HEPES buffer (pH 7.4), 7.5 mM $MgCl_2$, 0.1 mM dithiothreitol. The reaction was initiated with the addition of 200 nmol of NADPH. NADPH consumption was monitored for 5 min and calculated from the absorption changes at 340 nm using the extinction coefficient 6.22 mM^{-1} cm^{-1}. The reaction was then quenched with the addition of 10 μl of sulfuric acid. Each sample was divided into two 450-μl aliquots to which 6 nmol of cortexolone was added as an internal standard before extraction against 2 ml of dichloromethane. The samples were dried under nitrogen gas, resuspended in 70 μl of methanol, and loaded onto a Waters Nova-Pak C_{18} column (2.1 × 150 mm), with a flow rate of 0.5 ml/min and linear gradients of 90% buffer A, 95% water, 5% acetonitrile, 0.1% formic acid and 10% buffer B, 5% water, 95% acetonitrile, 0.1% formic acid to 40% buffer A at 15 min, 33% buffer A at 17 min, and isocratic flow of 33% buffer A to 40 min. TST and its metabolites were monitored at 240 nm, and concentrations were calculated using the extinction coefficient of 18.9 mM^{-1} cm^{-1} and confirmed by comparison with commercially available standards for 2β-, 6β-, and 15β-OH TST (16). ANF and its metabolites were monitored at 290 nm, and concentrations were calculated using the extinction coefficient of 23.7 mM^{-1} cm^{-1} (22). Standards for the ANF metabolites, the 7,8-dihydrodiol and 5,6-epoxide, were not commercially available, and their identification was surmised from published elution profiles and relative elution times (22, 23).

Data Fitting—Global analysis was performed as described previously (16) by simultaneously fitting the experimental data sets to the four-state linear Scheme 1, where E is the concentration of substrate-free CYP3A4, S is the concentration of unbound substrate, and ES_i is the concentration of the binding intermediates, complexes of CYP3A4 with i molecules of substrate bound ($i = 0, 1, 2, 3$).

The fractions of the enzyme substrate complexes were expressed using the standard binding polynomials (24),

$$Y = \frac{\frac{S}{K_1} + \frac{S^2}{K_1K_2} + \frac{S^3}{K_1K_2K_3}}{1 + \frac{S}{K_1} + \frac{S^2}{K_1K_2} + \frac{S^3}{K_1K_2K_3}} \quad \text{(Eq. 1)}$$

and the functional properties at different substrate concentrations were represented as the linear combination of the fractional contributions from binding intermediates. For example, the fraction of the high spin CYP3A4 in the Type I titrations, Y_S, is calculated as the weighted sum of the signals from the cytochrome P450 molecules with zero, one, two, or three substrate molecules bound, having a_0, a_1, a_2, and a_3 fractions of high spin state, correspondingly.

$$Y_S = \frac{a_0 + \frac{a_1S}{K_1} + \frac{a_2S^2}{K_1K_2} + \frac{a_3S^3}{K_1K_2K_3}}{1 + \frac{S}{K_1} + \frac{S^2}{K_1K_2} + \frac{S^3}{K_1K_2K_3}} \quad \text{(Eq. 2)}$$

The set of such equations for the spectral titration, NADPH consumption, and product formation has been used for the simultaneous fitting of the experimental data obtained under the same conditions, using the same set of dissociation constants, which yields a total of 12 parameters. The fitting program was written in MATLAB using the Nelder-Mead simplex minimization algorithm implemented in the subroutine "fminsearch.m."

The 10-state pyramidal binding model (Scheme 2) is used for an enzyme that can bind up to three total molecules of two different substrates. It is an extension of Scheme 1 that is incorporated along the outer pathways of Scheme 2. Binding

$$E + S \overset{K_1}{\leftrightarrow} ES_1 + S \overset{K_2}{\leftrightarrow} ES_2 + S \overset{K_3}{\leftrightarrow} ES_3$$

SCHEME 1

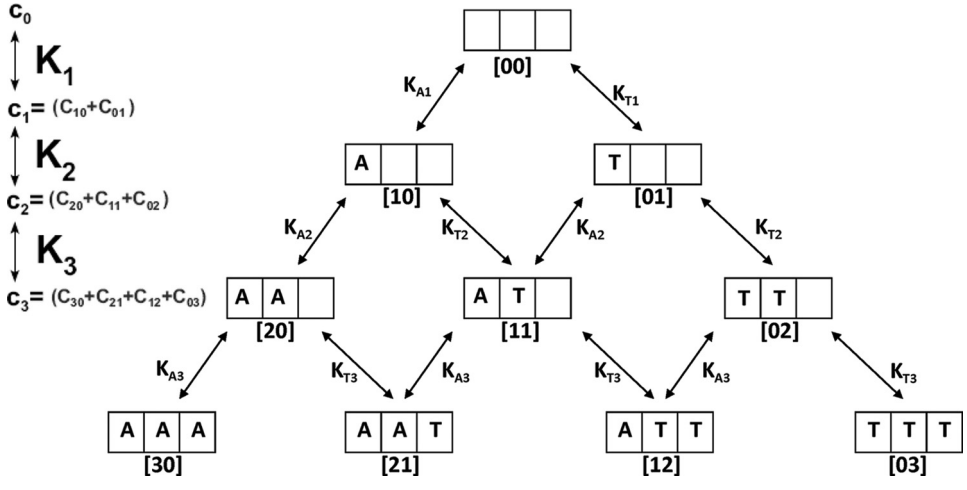

SCHEME 2

constants K_A and K_T, represent ANF and TST, respectively, and are the same for each binding step if there is an absence of intrinsic heterotropic cooperativity, *i.e.* binding of the next substrate molecule may depend on the presence of previously bound substrates ($K_{A1} \neq K_{A2}$). Scheme 2 also includes three mixed states where the enzyme interacts simultaneously with both substrates. In the case of a titration with a mixture of substrates at a constant substrate ratio, Scheme 2 can be formally represented by Scheme 1, where S is the total substrate in the system (here, A + T), and the mixed binding constants, K_i, are given by the average of the respective K_{Ai} and K_{Ti}, weighted against their molar ratio,

$$K_1 = \mu_A K_{A1} + \mu_T K_{T1} \quad \text{(Eq. 3)}$$

$$K_2 = \mu_A K_{A2} + \mu_T K_{T2} \quad \text{(Eq. 4)}$$

$$K_3 = \mu_A K_{A3} + \mu_T K_{T3} \quad \text{(Eq. 5)}$$

where μ_A and μ_T represent the molar fractions of ANF and TST, respectively. Thus each ratio of the two substrates can be represented by its own set of mixed binding constants and analyzed based upon the global analysis *versus* total substrate concentration, as if it were a single substrate. A detailed discussion of the equations used in the mixed substrate modeling is included in the supplemental material.

A Monte Carlo simulation was used to estimate the statistical errors of the fitted parameters as described (27, 28). A normally distributed random error was introduced into each fitted data set, using standard deviations of 2% for spin shift, 1 nmol/nmol/min for NADPH oxidation, and 0.1 nmol/nmol/min for product formation. A 67% confidence interval for each parameter value from the fits of 200 error-added data sets was used to estimate the error (25, 26).

RESULTS AND DISCUSSION

Global Analysis—Simultaneous fitting of the three observed enzyme properties, heme iron spin state, NADPH oxidation, and product formation for each substrate to a three-site binding model, shown in Scheme 1 (see "Experimental Procedures"), allowed for the deconvolution of the individual stepwise dissociation constants along with resolution of the fractional contributions of the binding intermediates to the overall behavior of the enzyme as a function of substrate concentration (Figs. 1 and 2 and Table 1, with errors estimated as described under "Experimental Procedures"). The low product-forming rate observed for ANF is likely due to the absence of cytochrome b_5, which has been reported to stimulate oxidation of this substrate (23). Attempts to fit the data for either substrate to a two-site nonspecific model failed, yielding negative values for one or more physiological parameters (data not shown). The properties of CYP3A4 follow similar trends for both ANF and TST, such as the fast acceleration and subsequent drop off in steady-state NADPH consumption with increasing substrate concentration. The binding of ANF is approximately one order of magnitude tighter than that of TST, with K_D values of 2, 3, and 7 μM and 27, 46, and 62 μM, respectively (Table 1). This leads to distinctions in the intermediate populations, which can account for the observed differences in enzyme properties. The binding of the first substrate molecule, forming the *E*S complex, increases the NADPH oxidation rate by severalfold for both substrates, to 182 nmol/nmol/min for TST and 106 nmol/nmol/min for ANF, although it does not induce product formation for either. For TST (22%), but not ANF (4%), this intermediate provides a small contribution to the spin shift. The binding of the second molecule of substrate forms the ES_2 complex, opens the product-forming pathway of the enzyme, and further stimulates the NADPH oxidation rate. For TST, both the NADPH oxidation rate and the product-forming rate are higher than for ANF (344 and 18 nmol/nmol/min for TST

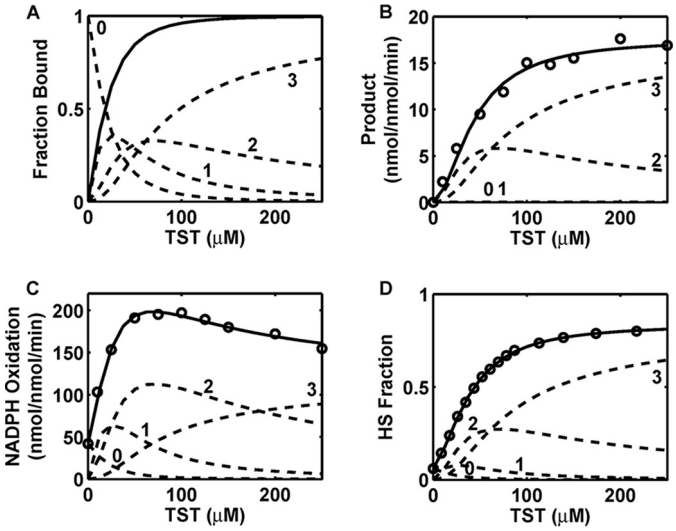

FIGURE 1. **Global analysis of TST binding.** The experimental data (*open circles*) for product formation (*B*), NADPH oxidation (*C*), and high spin (*HS*) fraction (*D*) were simultaneously fit to a three-site binding model, resulting in the global fit for each parameter (*solid lines*) and the overall binding saturation (*A*). The signal from each intermediate, with zero, one, two, or three TST molecules bound, is shown by the *dashed lines*.

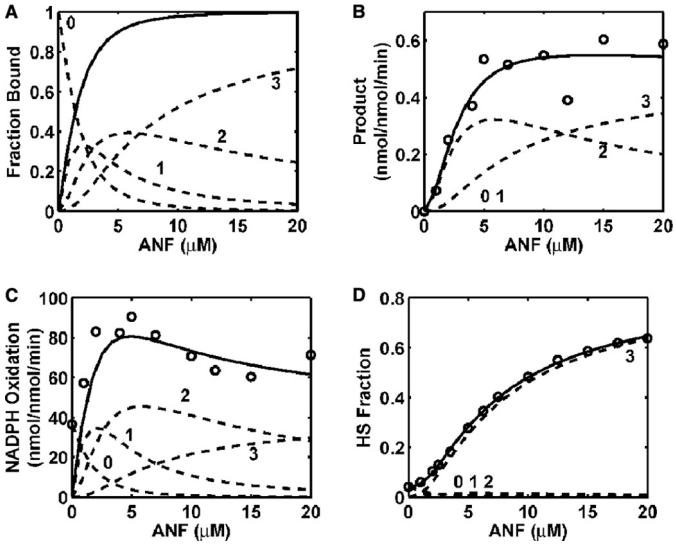

FIGURE 2. **Global analysis of ANF binding.** The experimental data (*open circles*) for product formation (*B*), NADPH oxidation (*C*), and high spin (*HS*) fraction (*D*) were simultaneously fit to a three-site binding model, resulting in the global fit for each parameter (*solid lines*) and the overall binding saturation (*A*). The signal from each intermediate, with zero, one, two, or three ANF molecules bound, is shown by the *dashed lines*.

TABLE 1

Parameters from single substrate global analyses

Confidence intervals are given in brackets below each fitted parameter. Dashes indicate the absence of error estimated from Monte-Carlo error analysis for the fixed parameters, which have been kept constant during fitting.

TST K_d (μM)			
	27 (23–35.5)	46 (38–52)	62 (52–77)
	Spin shift	**NADPH rate**	**Product-forming rate**
	%	*nmol/nmol/min*	*nmol/nmol/min*
E	6 ± 2.0	42 ± 1.0	0 ± 0.1
	—	—	—
ES	22 (17–32)	182 (159–224)	0 (0.01–0.06)
ES_2	83 (71–91)	344 (303–375)	18 (16.6–18.7)
ES_3	84 (80–88)	115 (112–120)	18 (17.3–17.8)
ANF K_d (μM)			
	2 (1.4–3.2)	3 (2.3–5.1)	7 (5–8.4)
	Spin shift	**NADPH rate**	**Product-forming rate**
	%	*nmol/nmol/min*	*nmol/nmol/min*
E	4 ± 2.0	36 ± 1.0	0 ± 0.1
	—	—	—
ES	4 (4–7.8)	106 (81–140)	0 (0–0.04)
ES_2	4 (3.8–7.0)	115 (89–122)	0.8 (0.55–1.24)
ES_3	89 (82–94)	41 (35–49)	0.5 (0.27–0.62)

and 115 and 0.8 nmol/nmol/min for ANF), and it correlates with a large shift to the high spin state. The ES_3 complex is formed with the binding of the third substrate molecule increasing the coupling efficiency (the ratio of the product formation to NADPH consumption) by decreasing NADPH consumption rather than stimulating product-forming rates. The third ANF binding also induces the Type I spin transition (89%), which is observed to occur at the second binding event for TST (83%). This observation is consistent with the characteristically higher apparent cooperativity of ANF, reflected in the Hill coefficient 1.7–2.2 (13, 27, 28) as compared with 1.3–1.6 documented for TST (16, 30, 31). The lack of product formation and negligible spin shift contributed from the *ES* complex provide an explanation for the apparent cooperativity of both functional properties.

In the absence of cooperativity, the stepwise dissociation constants should conform to the expected statistical ratio for the three-site binding model $K_1 = K_2/3 = K_3/9$ (Scheme 1) (29). The $\Delta\Delta G$ values between the sequential binding events can be calculated in comparison with the non-cooperative binding ratio where $\Delta\Delta G_{12} = -RT\cdot\ln(3\cdot K_1/K_2)$ and $\Delta\Delta G_{23} = -RT\cdot\ln(3\cdot K_2/K_3)$. For ANF, they are −0.4 and −0.2 kcal/mol, and for TST, they are −0.3 and −0.5 kcal/mol. These values are smaller than RT, 0.6 kcal/mol at room temperature, which means that there is virtually no deviation from purely statistical behavior for binding of these substrates. Because of essentially non-cooperative binding, the observed deviations from Michaelis-Menten behavior and apparently cooperative properties of the enzyme arise from differences in the fractional contributions of the enzyme-substrate complexes to their experimentally observed functional properties and are not due to an uneven distribution of the complexes themselves.

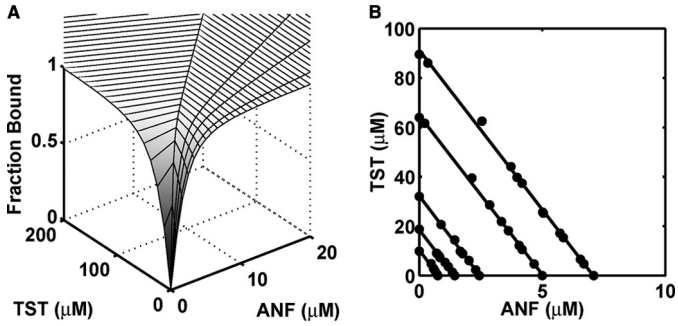

FIGURE 3. **Simulated non-cooperative binding surface (*A*) and contours (*B*) showing the 0.3, 0.5, 0.7, 0.9, and 0.95 saturation levels.** These results are based upon the linear combination of the fitted binding isotherms of ANF and TST.

Mixed Substrate Analysis—Building upon the linear four-state binding models (Scheme 1) for each substrate, a 10-state pyramidal model was developed to account for a mixed substrate system in which CYP3A4 can accommodate up to three molecules of either substrate into the active site (Scheme 2). The stepwise binding constants for ANF and TST along with functional amplitudes for the outer non-mixed states are given through a global analysis of each substrate (Table 1). For the three mixed states, the average values of the non-mixed amplitudes derived from the homotropic global fits have been used as it is impossible to directly measure these properties. Because this model is based upon the linear combination of the global fits of each substrate, it represents a system without any specific heterotropic cooperativity but intrinsically includes the homotropic cooperativity of each substrate if present. This is apparent from the simulated binding surface contours (Fig. 3*B*), which are linear, indicating that substrate saturation levels are being reached at the same relative substrate concentrations in mixed or single-substrate titrations. Positive or negative heterotropic cooperativity results in the saturation contours curving toward or away from the origin, respectively (17).

To test the possible effect of heterotropic interactions, a 1:3 ANF:TST titration was simulated with ±0.6 kcal/mol of cooperativity for each of the three mixed intermediates and compared with the observed data for each of the three functional properties (Fig. 4). The effect of introduced heterotropic interactions on the spin shift is apparent only at lower substrate concentrations. This is explained by examining the intermediate populations for simulated cooperativity (Fig. 5). Positive heterotropic interactions skew the populations of enzyme-substrate complexes toward the saturated mixed states, whereas negative interactions have the opposite effect. The contribution from the *ES* complex is increased in simulated negative (Fig. 5*A*) interactions relative to positive ones (Fig. 5*B*). The contribution of the ES_2 complex increases at lower substrate concentrations in the presence of the simulated positive heterotropic interactions. Even in the presence of negative interactions, the contribution of the ES_3 complex is so dominant at high substrate concentrations that the effects of simulated heterotropic cooperativity are minimized in this region.

As seen from Fig. 4, the heterotropic interactions would show the largest effect on product formation if present. This

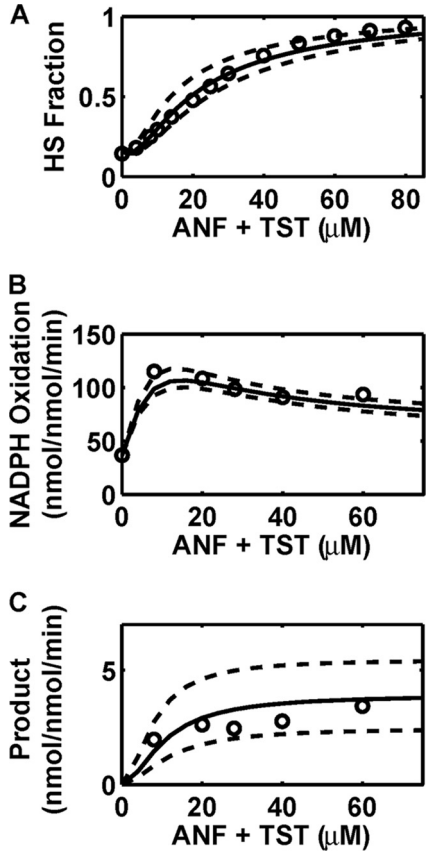

FIGURE 4. **1:3 ANF:TST mixed titration.** Experimental data (*open circles*) for each of the functional properties are compared with the simulations in the absence of heterotropic interactions (*solid lines*) and with positive and negative 0.6 kcal/mol of heterotropic interactions (*top* and *bottom dashed lines*, respectively). *HS*, high spin.

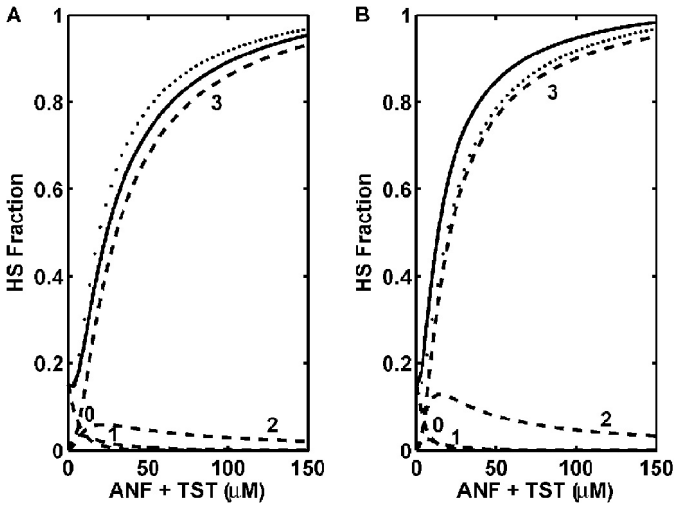

FIGURE 5. **Simulated fractional contributions from the intermediates for 1:3 mixed ANF:TST titration monitored by the spin shift, negative heterotropic cooperativity (*A*), and positive heterotropic cooperativity (*B*) of 0.6 kcal/mol.** The signal from each intermediate in the simulation, with zero, one, two, or three substrate molecules bound, is shown by the *dashed lines*. The overall signal is given by the *solid line*, and the non-cooperative reference is shown by the *black dots*. *HS*, high spin.

is due to the fact that the product formation is dominated evenly by contributions from the ES_2 and ES_3 complexes, which encompass the mixed substrate complexes where heterotropic interactions are maximized. The effects of the added heterotropic cooperativity for NADPH oxidation are muted due to the larger contribution of the *E*S complex and smaller contribution of the ES_3 complex to the overall oxidation rate, relative to product formation.

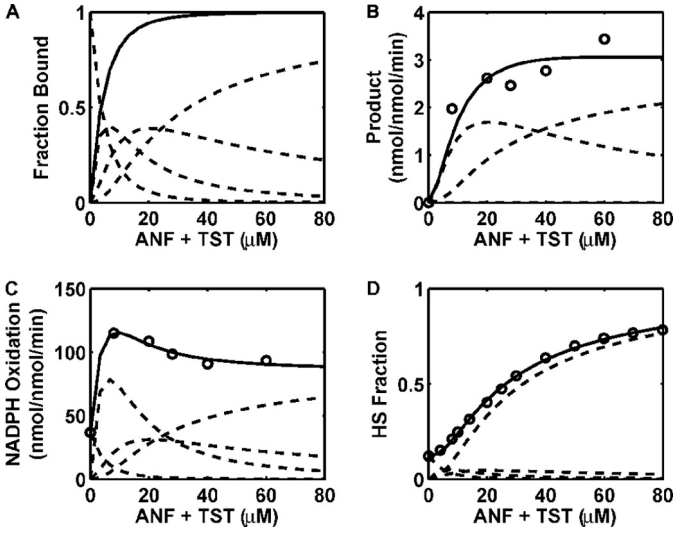

FIGURE 6. **Global fitting of 1:3 ANF:TST data sets.** The experimental data (*open circles*) for product formation (*B*), NADPH oxidation (*C*), and high spin (*HS*) fraction (*D*) were simultaneously fit to a three-site binding model, resulting in the global fit for each parameter (*solid lines*) and the overall binding saturation (*A*). The signal from each intermediate, with zero, one, two, or three substrate molecules bound is shown by the *dashed lines*.

TABLE 2

Parameters from mixed substrate global analysis

Confidence intervals are given in brackets. Dashes indicate the absence of error estimated from Monte-Carlo error analysis for the fixed parameters, which have been kept constant during fitting.

1:3 mix K_d (μM)	5 (2–6)	12 (12–19)	24 (19–24)
	Spin shift	**NADPH rate**	**Product-forming rate**
	%	*nmol/nmol/min*	*nmol/nmol/min*
E	12 ± 2.0	37 ± 1.0	0 ± 0.1
	—	—	—
ES	13 (11.7–14.3)	195 (149–205)	0 (0–0.01)
ES_2	12 (11.7–14.1)	80 (54–90)	4 (4–5.6)
ES_3	103 (100)[a]	87 (82–92)	3 (2.3–3)

[a] Constrained.

Mixed Global Analysis—As was done with the single-substrate data sets for spin transition, NADPH oxidation, and product formation, the mixed 1:3 ANF:TST data sets were also fit to a three-site nonspecific binding model, which allows deconvolution of the stepwise binding constants as a function of total substrate concentration for the particular substrate ratio (Fig. 6). The apparent dissociation constants of 5, 12, and 24 μM (Table 2, with errors estimated as described under "Experimental Procedures") fall in between those of ANF and TST, and calculating the $\Delta\Delta G$ values between the binding events gives −0.1 and −0.2 kcal/mol of heterotropic cooperativity, confirming the results of the simulation that there is no heterotropic cooperativity in the system. The same trends are followed for the mixed substrate system that were observed for each of the functional properties in both single-

substrate systems, such as the lack of product formation coming from the *E*S complex and the inhibition of NADPH oxidation at higher substrate concentrations.

Although binding of the first substrate triggers an increase in NADPH oxidation, it is entirely uncoupled, and a second substrate molecule must bind for the product-forming pathway to open. The third binding event does not significantly alter the rate of product formation but does decrease the NADPH oxidation rate, increasing the coupling efficiency of the P450 cycle. This indicates that the apparently synergistic functional interactions between ANF and TST are not due to their heterotropic interactions and binding cooperativity but rather reflect the differences in the fractional contributions of the various enzyme-substrate complexes, which give rise to the overall functional properties.

Conclusions—The addition of either ANF or TST to the system of CYP3A4 in Nanodiscs drives the population of enzyme-substrate complexes toward the more fully saturated, and catalytically productive, states. The minor contribution of the single-substrate-bound complex (*E*S) to the spin state transition and product formation causes the appearance of homotropic or heterotropic cooperativity for these properties, although the binding events are actually occurring non-cooperatively, *i.e.* with no interaction free energy. Using the spin state shifts for the individual substrates, ANF and TST, it is possible to accurately simulate the spin shift for a given ratio of the two substrates. This indicates that any apparent cooperativity in the mixed substrate system is equivalent to the sum of the contributions of the apparent homotropic cooperativity of each substrate. Analysis of the functional properties of CYP3A4 in the mixed substrate ANF-TST system reveals the absence of any specific heterotropic interactions between these substrates, in complete agreement with our previous results for spin shift based upon the Hill model (17). The global analysis of each substrate provides a detailed description of the landscape of the homotropic interactions. Together these descriptions are used to define the reference state for the mixed substrate system in the absence of heterotropic cooperativity, which is then compared with the observed behavior when two substrates are present. The experimental data for the mixed titrations are nearly identical to those predicted by the non-cooperative reference system. This clearly demonstrates that the mixed substrate system is accurately described by the additive effects of the two single-substrate titrations and indicates negligible binding cooperativity between ANF and TST.

Acknowledgments—We gratefully acknowledge Y. V. Grinkova for help and advice and other members of the S. G. Sligar laboratory for useful discussions.

REFERENCES

1. Shimada, T., Yamazaki, H., Mimura, M., Inui, Y., and Guengerich, F. P. (1994) *J. Pharmacol. Exp. Ther.* **270,** 414–423
2. Wienkers, L. C., and Heath, T. G. (2005) *Nat. Rev. Drug Discov.* **4,** 825–833
3. Shou, M., Grogan, J., Mancewicz, J. A., Krausz, K. W., Gonzalez, F. J., Gelboin, H. V., and Korzekwa, K. R. (1994) *Biochemistry* **33,** 6450–6455
4. Atkins, W. M. (2005) *Annu. Rev. Pharmacol. Toxicol.* **45,** 291–310
5. Davydov, D. R., and Halpert, J. R. (2008) *Expert Opin. Drug Metabol. Toxicol.* **4,** 1523–1535
6. Guengerich, F. P. (2005) in *Cytochrome P450: Structure, Mechanism, and Biochemistry* (Ortiz de Montellano, P. R., ed) pp. 337–530, 3rd Ed., Kluwer Academic/Plenum Publishers, New York
7. Ekroos, M., and Sjögren, T. (2006) *Proc. Natl. Acad. Sci. U.S.A.* **103,** 13682–13687
8. Williams, P. A., Cosme, J., Vinkovic, D. M., Ward, A., Angove, H. C., Day, P. J., Vonrhein, C., Tickle, I. J., and Jhoti, H. (2004) *Science* **305,** 683–686
9. Schwab, G. E., Raucy, J. L., and Johnson, E. F. (1988) *Mol. Pharmacol.* **33,** 493–499
10. Atkins, W. M. (2006) *Expert Opin. Drug Metab. Toxicol.* **2,** 573–579
11. Harlow, G. R., and Halpert, J. R. (1998) *Proc. Natl. Acad. Sci. U.S.A.* **95,** 6636–6641
12. Shou, M., Dai, R., Cui, D., Korzekwa, K. R., Baillie, T. A., and Rushmore, T. H. (2001) *J. Biol. Chem.* **276,** 2256–2262
13. Tsalkova, T. N., Davydova, N. Y., Halpert, J. R., and Davydov, D. R. (2007) *Biochemistry* **46,** 106–119
14. Denisov, I. G., Frank, D. J., and Sligar, S. G. (2009) *Pharmacol. Ther.* **124,** 151–167
15. Sligar, S. G., and Denisov, I. G. (2007) *Drug Metab. Rev.* **39,** 567–579
16. Denisov, I. G., Baas, B. J., Grinkova, Y. V., and Sligar, S. G. (2007) *J. Biol. Chem.* **282,** 7066–7076
17. Frank, D. J., Denisov, I. G., and Sligar, S. G. (2009) *Arch. Biochem. Biophys.* **488,** 146–152
18. Baas, B. J., Denisov, I. G., and Sligar, S. G. (2004) *Arch. Biochem. Biophys.* **430,** 218–228
19. Grinkova, Y. V., Denisov, I. G., and Sligar, S. G. (2010) *Biochem. Biophys. Res. Commun.* **398,** 194–198
20. Denisov, I. G., and Sligar, S. G. (2011) *Biochim. Biophys. Acta* **1814,** 223–229
21. Nath, A., Grinkova, Y. V., Sligar, S. G., and Atkins, W. M. (2007) *J. Biol. Chem.* **282,** 28309–28320
22. Ueng, Y. F., Kuwabara, T., Chun, Y. J., and Guengerich, F. P. (1997) *Biochemistry* **36,** 370–381
23. Borek-Dohalska, L., and Stiborova, M. (2010) *Collect. Czech. Chem. Comm.* **75,** 201–220
24. DiCera, E. (1995) *Thermodynamic Theory of Site-Specific Binding Processes in Biological Macromolecules*, Cambridge University Press, Cambridge, UK
25. Tellinghuisen, J. (2009) *Methods Enzymol.* **467,** 499–529
26. Straume, M., and Johnson, M. L. (1992) *Methods Enzymol.* **210,** 117–129
27. Domanski, T. L., He, Y. A., Harlow, G. R., and Halpert, J. R. (2000) *J. Pharmacol. Exp. Ther.* **293,** 585–591
28. Hosea, N. A., Miller, G. P., and Guengerich, F. P. (2000) *Biochemistry* **39,** 5929–5939
29. Klotz, I. M. (1997) *Ligand-Receptor Energetics: A Guide for the Perplexed*, John Wiley & Sons, Inc., New York
30. Isin, E. M., and Guengerich, F. P. (2006) *J. Biol. Chem.* **281,** 9127–9136
31. Kenworthy, K. E., Clarke, S. E., Andrews, J., and Houston, J. B. (2001) *Drug Metab. Dispos.* **29,** 1644–1651